

# FRactal Grid Turbulence and Acoustic Predictions

S. Laizet<sup>a</sup>, V. Fortuné<sup>b</sup>, E. Lamballais<sup>b</sup> and J.C. Vassilicos<sup>a</sup>

<sup>a</sup>Turbulence, Mixing and Flow Control Group,  
Department of Aeronautics, Imperial College London  
London, SW7 2BY, United Kingdom

<sup>b</sup>Department of Fluid Flow, Heat Transfer and Combustion, Institute PPRIME  
CNRS - Université de Poitiers - ENSMA  
Téléport 2, Boulevard Marie et Pierre Curie, BP 30179  
86962 Futuroscope Chasseneuil Cedex, France

## ABSTRACT

In this numerical work, we compare the acoustic properties of a fractal square grid with those of a regular grid by means of a hybrid approach based on Lighthill's analogy and Direct Numerical Simulation (DNS). It has been shown that the turbulence generated by fractal objects can have different properties than those generated by a regular object: whereas a regular object effectively introduces a single length-scale into the flow, a fractal object can introduce a wide range of length-scales into the flow. These distinct turbulent states depending on the grid are found to lead to different acoustic radiations both in terms of sound pressure levels and frequencies.

## INTRODUCTION

A promising noise reduction concept based on multiscale flow profilers/shapers such as fractal grids has been studied experimentally in Poitiers (France) and Imperial College London (UK) [1, 2]. This new noise reduction concept arose from recent research on turbulence generated by fractal grids in a wind tunnel [3, 4]. Indeed, flows generated by multiscale grids have some very unusual properties which could be interesting for noise reduction. The aim of this work is to investigate via DNS the acoustic field generated by a fractal grid in order to check its noise reduction potential. A fractal square grid and a regular grid (see figure 1) of equal blockage ratio are investigated and compared in order to capture the influence of the shape of the grid on the acoustic field, but also to attempt to understand how the acoustic field is modified when it is generated at different scales. This numerical study follows experimental measurements undertaken in an anechoic chamber in Poitiers and in an aeroacoustic wind tunnel in Braunschweig (Germany) in the framework of the OPENAIR project, a European Commission initiative. In these experiments, a reduction in sound pressure levels was obtained at low frequencies, while an increase in sound pressure levels was obtained at high frequencies, and overall, a slight reduction in sound pres-

sure levels was indeed recorded with fractal spoilers relative to solid and regular grid spoilers. It should be interesting to check if such a behaviour can be reproduced numerically.

Identifying the mechanisms responsible for the production of sound by turbulent flows remains to date an extremely difficult task, even for very extensively studied problems, like jet noise. Experimental studies are generally not sufficient when knowledge about the physical mechanisms of noise production is required. DNS allow the calculation of all unsteady flow quantities and can help us to investigate the aerodynamically generated sound. The direct computation of sound by solving the compressible Navier Stokes equations provides both the aerodynamic field and the acoustic field simultaneously [5–7], but the very high cost of this direct approach is still a limiting factor. In consequence, flow-generated acoustic fields are often predicted via a hybrid approach [8, 9], using acoustic analogies or wave extrapolation methods.

In the present work, DNS of turbulent flows generated by a regular and a fractal grids are carried out [10], thanks to an efficient parallel solver called **Incompact3d** for the incompressible Navier-Stokes equations [11–13]. Then the acoustic radiation from the flow across the grids is evaluated thanks to a hybrid approach based on the Lighthill acoustic analogy.

## FLOW SIMULATIONS

The objective of present simulations is to obtain the instantaneous databases necessary to evaluate the acoustic sources from the turbulent flow through the grids, in order to investigate their associated sound radiation. In this numerical study, we are interested in two turbulent flows generated by two grids: one regular grid and one fractal square grid (see figure 1). The streamwise upstream velocity  $U_\infty$  is uniform in all cases with no turbulence. Unlike the regular grid, the fractal grid does not have a well-defined mesh size. [3] introduced an effective mesh size  $M_{eff} = \frac{4T^2}{P} \sqrt{1 - \sigma}$  where  $P$  is the perimeter length of the fractal grid,  $T$  the lateral size of

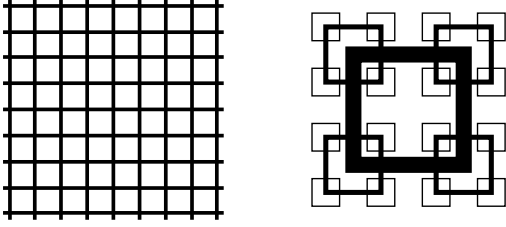


Figure 1. Scaled diagrams of the two different grids used in this numerical study: a regular grid (left) and a fractal square grids with an aspect ratio  $t_r$  of 8.5 (right), where  $t_r$  is the ratio between the biggest and smallest lateral thicknesses.

the wind tunnel and  $\sigma$  the blockage ratio. When applied to a regular grid,  $M_{eff}$  equals the actual mesh size of the grid. The simulations are performed with the same Reynolds number (based on  $U_\infty$  and  $M_{eff}$ )  $Re_{M_{eff}} = 4500$ , same blockage ratio ( $\sigma = 0.25$ ) and same effective mesh size ( $M_{eff} = 15.4t_{min}$ , where  $t_{min}$  is the size of the smallest lateral thickness of the fractal grid). Note that the thickness of the bars for the regular grid is  $2.6t_{min}$ . Each turbulent flow governed by the incompressible Navier-Stokes equations is considered in Cartesian coordinates  $x_i = (x, y, z)$ . To solve these equations, we use **Incompact3d** based on sixth-order compact schemes for spatial discretization and a third order Adams-Bashforth scheme for time advancement. To treat the incompressibility condition, a fractional step method requires to solve a Poisson equation. This equation is fully solved in spectral space, via the use of relevant 3D Fast Fourier Transforms. The pressure mesh is staggered from the velocity mesh by half a mesh, to avoid spurious pressure oscillations. With the help of the concept of modified wave number, the divergence free condition is ensured up to machine accuracy. More details about the present code and its validations, especially the original treatment of the pressure in spectral space, can be found in [11]. The modelling of the grids is performed by an Immersed Boundary Method. The present method is a direct forcing approach that ensures the no-slip boundary condition at the grid walls. Because of the size of the simulations, the parallel version of **Incompact3d** has been used. Based on a highly scalable 2D decomposition library and a distributed FFT interface, it is possible to use the code on thousands of computational cores. More details about this efficient parallel strategy can be found in [13].

The computational domain is  $L_x \times L_y \times L_z = 460.8t_{min} \times 115.2t_{min} \times 115.2t_{min}$  discretized on a Cartesian mesh of  $n_x \times n_y \times n_z = 2305 \times 576 \times 576$  mesh nodes. It is split in 3,456 computational cores. Inflow/outflow boundary conditions are used in the  $x$ -direction and periodic boundary conditions in the  $y$ - and  $z$ -directions. The time step  $\Delta t = 0.015t_{min}/U_\infty$  is low enough to have a CFL condition of about 0.75. The streamwise position of the grids ( $10t_{min}$ ) from the inlet boundary of the computational domain has been carefully chosen to avoid any spurious interactions between the modelling of the grid and the inflow boundary condition. An illustration of the flow obtained in both cases is given in figure 2, in which enstrophy isosurfaces are plotted. These isosurfaces are normalised in such a way that the decay of the turbulence is not visible on these plots. The one obvious difference in these visualiza-

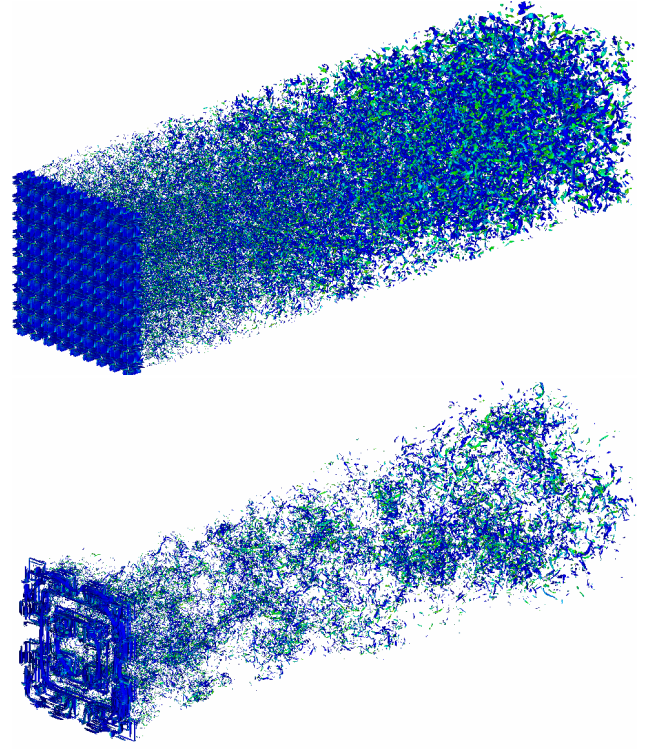


Figure 2. Turbulent flows generated by the regular grid (top) and by the fractal grid (bottom). Specifically, 3D isosurfaces of (in blue) the absolute value of the vorticity vector normalised by its maximum over the  $y$ - $z$  plane at the  $x$ -position considered, and of (in green) the  $x$ -component of the vorticity normalised by its maximum over the  $y$ - $z$  plane at the  $x$ -position considered. The value on both isosurfaces is 0.7.

tions between the turbulent flow generated by the regular grid and the turbulent flow generated by the fractal square grid is that the latter is clearly more intermittent. The fact is also that these two different types of turbulent flows are generated in different ways. In the regular grid case, same-size wakes interact within a couple of mesh sizes from the grid and mix together in a uniform fashion close to the grid. In the fractal grid case, [4, 10, 14] suggested that the smallest bars on the grid generate the smallest wakes which meet and mix together at the smallest distance from the grid, whereas larger bars generate larger wakes which meet and mix at a further distance from the grid, and that this process repeats itself from the smallest to the largest turbulence-generating scales on the grid in a way which causes the turbulence to progressively intensify over a protracted distance from the grid. Following this turbulence generation mechanism, the turbulence decay for both grids is clearly visible in figure 3 where we plot the maximum of the turbulent kinetic energy  $k_{max}$  over every  $(y-z)$  plane as a function of the streamwise coordinate  $x$ . It is clear from this figure that the present fractal grid generates higher turbulent kinetic energy than the regular grid, even very close to the grid.

One can also see in figure 4 how  $u'/U_\infty$  peaks at different streamwise locations along streamwise lines crossing the

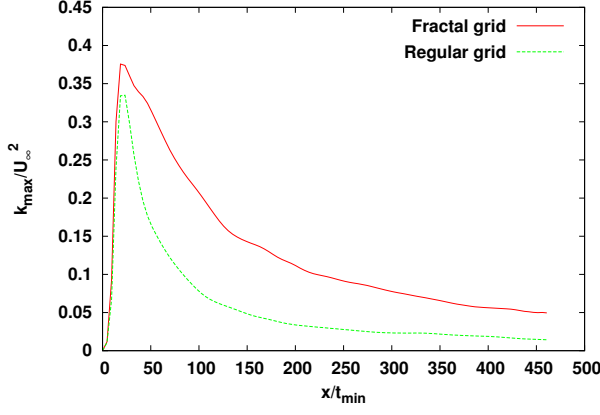


Figure 3. Streamwise evolution of the maximum of the turbulent kinetic energy for the two grids.

grid at different lateral locations for both grids. For the fractal square grid, there are clear wake-like behaviours where this location is on a blocking bar and more jet-like behaviours where this location is on an empty region of the grid. It is also clear from this picture that the furthest peak point is the one on the centreline. For the regular grid, we observe differences in the turbulence production region very close to the grid but nevertheless a similar behaviour for  $u'/U_\infty$  after  $x/t_{min} \approx 75$  where the turbulent flow is quasi-homogeneous.

In the following, we are interested in investigating the sound production associated with the turbulent flow for both grids. In particular, we will see whether the differences in behaviour of flow structures which we have just highlighted involve or not differences on the acoustic field.

## METHODOLOGY FOR ACOUSTIC PREDICTION

The acoustic fields generated by the flow across each grid are evaluated via a hybrid approach based on the Lighthill analogy [15]. Lighthill's equation is an exact reformulation of the Navier-Stokes equations in order to obtain an inhomogeneous wave equation describing the sound generated in a medium at rest by the fluctuating stresses embedded in a localised domain, called the source domain. The associated solution can be obtained with the use of a Green function. Because in our configuration the source domain also involves solid boundaries, the Curle formulation [16] of the integral solution is used, based on the acoustic pressure  $p_a$  in the ambient medium, at the observer position  $\mathbf{x}$  and the time  $t$ . It can be expressed as

$$\begin{aligned}
 p_a(\mathbf{x}, t) = & \frac{1}{4\pi} \frac{\partial^2}{\partial x_i \partial x_j} \int_V T_{ij} \left( \mathbf{y}, t - \frac{|\mathbf{x} - \mathbf{y}|}{c_0} \right) \frac{dV}{|\mathbf{x} - \mathbf{y}|} \quad (1) \\
 & - \frac{1}{4\pi} \frac{\partial}{\partial t} \int_S \rho u_i \left( \mathbf{y}, t - \frac{|\mathbf{x} - \mathbf{y}|}{c_0} \right) n_i \frac{dS}{|\mathbf{x} - \mathbf{y}|} \\
 & + \frac{1}{4\pi} \frac{\partial}{\partial x_i} \int_S (\rho u_i u_j + p \delta_{ij} - \tau_{ij}) \left( \mathbf{y}, t - \frac{|\mathbf{x} - \mathbf{y}|}{c_0} \right) n_i \frac{dS}{|\mathbf{x} - \mathbf{y}|}
 \end{aligned}$$

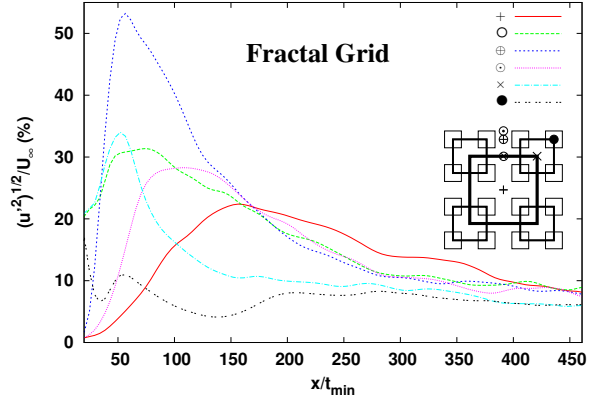
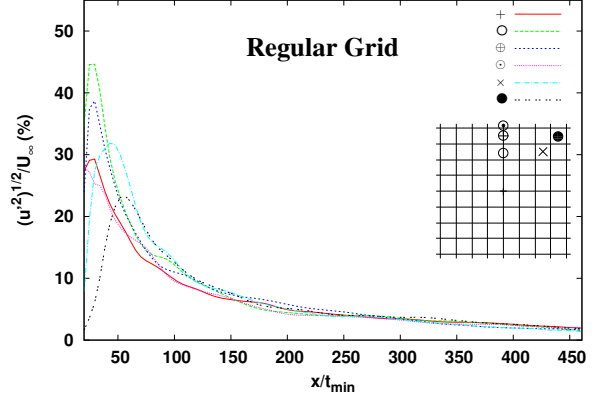


Figure 4. Streamwise evolution of  $(u'^2)^{1/2}/U_\infty$  at different lateral locations for the four simulations: + corresponds to  $y/t_{min} = 0, z/t_{min} = 0$ ,  $\times$  to  $y/t_{min} = 28.8, z/t_{min} = 28.8$ ,  $\bullet$  to  $y/t_{min} = 43.2, z/t_{min} = 43.2$ ,  $\otimes$  to  $y/t_{min} = 0, z/t_{min} = 28.8$ ,  $\oplus$  to  $y/t_{min} = 0, z/t_{min} = 43.2$  and  $\odot$  to  $y/t_{min} = 0, z/t_{min} = 50.4$ .

where  $p$  is the pressure,  $\rho$  the density,  $\mathbf{u}$  the velocity field in the source domain  $V$ ,  $S$  the surface of the solid boundaries and  $\mathbf{n}$  the outward normal from the fluid.  $T_{ij} = \rho u_i u_j + (p - c_0^2 \rho) \delta_{ij} - \tau_{ij}$  is the Lighthill source term, where  $\tau_{ij}$  are the viscous stresses and  $c_0$  is the sound velocity in the ambient medium. The viscous contribution is negligible for flows with relatively high Reynolds numbers, and the approximated value of the Lighthill source term  $T_{ij} \approx \rho u_i u_j$  is generally retained, for isothermal flows at low Mach numbers. Note that the source quantities in the integrands of equation (1) have to be evaluated at retarded times  $t - |\mathbf{x} - \mathbf{y}|/c_0$ .

For a far field location at an observer point ( $|\mathbf{x}| \gg |\mathbf{y}|$ ),

[16] showed that (1) can be approximated by

$$p_a(\mathbf{x}, t) = \frac{1}{4\pi c_0^2} \frac{x_i x_j}{|\mathbf{x}|^3} \frac{\partial^2}{\partial t^2} \int_V [T_{ij}] dV \quad (2)$$

$$- \frac{1}{4\pi} \frac{1}{|\mathbf{x}|} \frac{\partial}{\partial t} \int_S [\rho u_i] n_i dS \quad (3)$$

$$- \frac{1}{4\pi c_0} \frac{x_i}{|\mathbf{x}|^2} \frac{\partial}{\partial t} \int_S [\rho u_i u_j + p \delta_{ij}] n_i dS \quad (4)$$

where [...] denotes the fact that the source quantities are evaluated at retarded times.

As stated by [16], the sound field can be viewed as the sum of three contributions: (i) the volume integral corresponding to (2) representing the effects of the hydrodynamic fluctuations included in the flow domain; (ii) the first surface integral corresponding to (3) representing the effect of flow rate fluctuations through the surface; and (iii) the second surface integral corresponding to (4) representing a flux of momentum and pressure through the surface. If there is zero normal velocity at the surface, only the surface integral associated with the pressure remains. If no solid boundaries are embedded in the flow domain, only the volume integral remains, like in the classical Lighthill theory.

From the equation of the acoustic pressure, dimensional analysis can be carried out in order to evaluate the scaling of the acoustic intensity  $I$  with the acoustic Mach number of the flow. It is showed in [15] that the volume integral contribution (2) induces a scaling of  $I$  as  $M^8$ , while the surface contributions associated with (3) and (4) induce scalings of  $I$  as  $M^4$  and  $M^6$  respectively. In the present configuration of grid-generated turbulence, we consider only a flow at low Mach number, so the contributions of the surface integrals are expected to be dominant. We follow an approach successfully used to predict previously the sound radiated by a flow around a cylinder (see figure 5) and consider a control surface  $S$  surrounding the actual solid surface of the grid (because the latter is very complex to define accurately). In such case where a shifted control surface  $S$  is used, the contributions of momentum flux through the control surface have to be retained. Furthermore, the surface integral associated with the flow rate is zero because the flow is stationary upstream of the grid. Hence the formulation that we have retained here to estimate the acoustic pressure is only based on the surface integral (4). It is important to note at this point that the present methodology based on the estimation of surface integrals accounts actually for the sound generation by the turbulent flow itself. In fact the surface integrals are not the actual physical sources of sound, but represent the diffraction by the solid surface of the sound generated by the turbulent flow. It is well known that the diffraction process is the main contributor to the sound production, for a flow at low Mach number, as shown by [17] in the case of the sound radiated by a flow around a cylinder.

The acoustic pressure in our flow configuration is obtained from the surface data recorded at two planes  $S_1 / S_2$ , located at one mesh node before/after the grid. The final formulation of the acoustic pressure that we use in the present

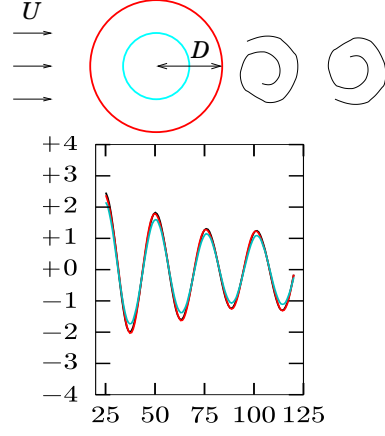


Figure 5. *Acoustic prediction of the sound generated by the flow around a circular cylinder of diameter  $D$ , based on the surface integrals of Curle's formulation (equation 4). At top, flow configuration and surfaces used as control surfaces (solid surface in cyan, shifted surface with a shift of  $D/2$  in red); at bottom, acoustic pressure signals vs. distance of the cylinder centre obtained by using the solid surface as control surface in cyan, and that obtained by using the shifted surface as control surface in red.*

work can be expressed as

$$\begin{aligned} -4\pi c_0 p_a(\mathbf{x}, t) = & \frac{X}{R^2} \left\{ \int_{S_1} \left[ \frac{\partial p}{\partial t} \right] dS - \int_{S_2} \left[ \frac{\partial p}{\partial t} \right] dS \right\} \\ & + \frac{X}{R^2} \left\{ \int_{S_1} \left[ \frac{\partial \rho u_x u_x}{\partial t} \right] dS - \int_{S_2} \left[ \frac{\partial \rho u_x u_x}{\partial t} \right] dS \right\} \\ & + \frac{Y}{R^2} \left\{ \int_{S_1} \left[ \frac{\partial \rho u_x u_y}{\partial t} \right] dS - \int_{S_2} \left[ \frac{\partial \rho u_x u_y}{\partial t} \right] dS \right\} \\ & + \frac{Z}{R^2} \left\{ \int_{S_1} \left[ \frac{\partial \rho u_x u_z}{\partial t} \right] dS - \int_{S_2} \left[ \frac{\partial \rho u_x u_z}{\partial t} \right] dS \right\} \quad (5) \end{aligned}$$

with  $(X, Y, Z)$  the coordinates of the observer point and  $R = \sqrt{X^2 + Y^2 + Z^2}$ . The computational estimations of the corresponding integrals have to be carried out carefully so as to take into account the difference in propagation distance between two source points because their respective contributions must be collected at different emission times so that they reach the observer point at the same time. It is therefore necessary to perform interpolations of the source fields known at discrete points and times to obtain the values at the exact position and time imposed by the integrals at retarded times. The results presented in the following section are obtained with the aid of an optimised acoustic algorithm which was developed to give access to acoustic fields generated by unsteady flows [18]. It is based on an advanced time approach [19] and an iterative selection of source-observer pairs involved in the sound generation process at a given time-step. It has already been used to compute successfully the sound radiated by a turbulent mixing layer [18] and a turbulent wake behind a cylinder [20].

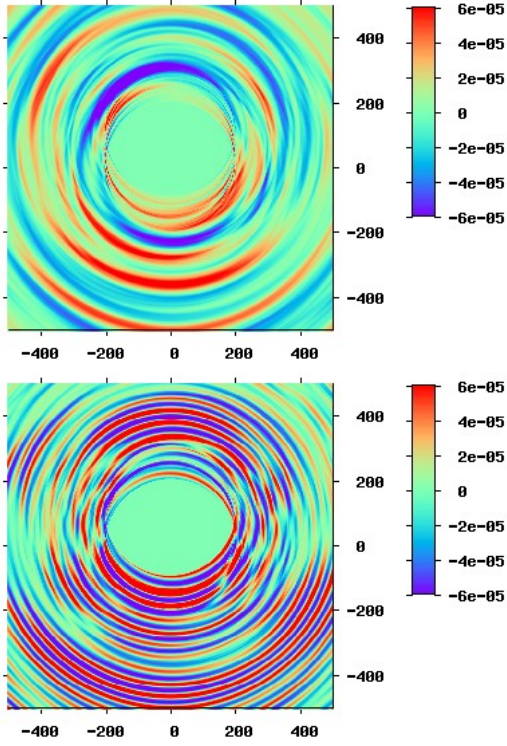


Figure 6. Acoustic pressure fields generated by the regular grid at top and by the fractal grid at bottom, in the observer plane ( $-500 t_{min} < X < 500 t_{min}$ ,  $-500 t_{min} < Y < 500 t_{min}$ ,  $Z = 0$ ), at the observer time  $t = 81 t_{min}/U_{\infty}$ . The centre of the regular/fractal grids is located at  $(0, 57.2 t_{min}, 0)$ .

## ACOUSTIC RESULTS

In this section, the procedure presented in the previous section is applied to compute the acoustic fields radiated by the grid flows. From the simulation of each flow, 667 source fields in the two surfaces  $S_1$  and  $S_2$  located at one mesh nodes before and after the grids respectively are stored during  $150 t_{min}/U_{\infty}$ . Our acoustic predictions are made for a flow with a Mach number  $M = U_{\infty}/c_0 = 0.1$ . First the acoustic fields radiated in an observer plane located at  $Z = 0$  are computed. The observer plane of size  $1000 t_{min} \times 1000 t_{min}$  contains  $10^6$  mesh nodes. Examples at a given observer time of the acoustic pressure fields obtained are shown in figure 6 for the regular and fractal grids. We note differences between both fields, in particular in terms of acoustic wavelengths: about 4 / 10 wavefronts are observed in the case of the flow generated by the regular / fractal grid respectively. The wave amplitudes are also slightly larger for the fractal square grid by comparison with the regular grid.

Figures 7 and 8 show the time evolution of the acoustic pressure at the same observer location for both cases. As in figure 6, we observe that the time period of the pressure signal is larger in the case of the regular grid than in the case of the fractal grid. In these figures the contributions of the terms associated with the pressure and with the momentum flux are also shown. We notice that the contribution associated with the momentum flux is dominant in the case of the flow gen-

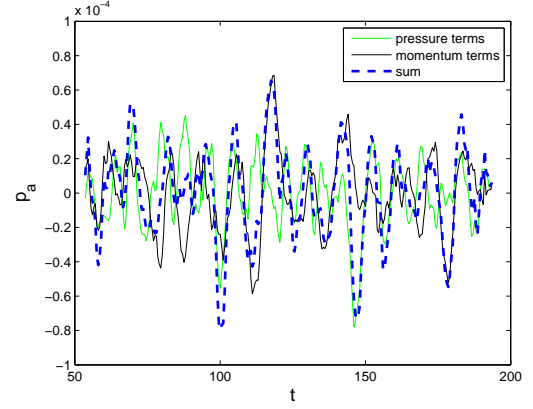


Figure 7. Time evolution of the acoustic pressure at the observer location  $(250 t_{min}, 433 t_{min}, 0)$  for the regular grid.

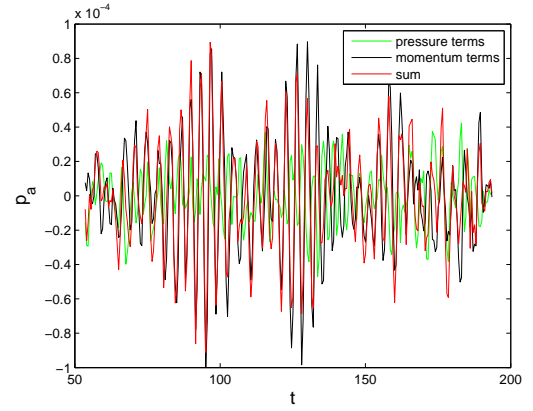


Figure 8. Time evolution of the acoustic pressure at the observer location  $(250 t_{min}, 433 t_{min}, 0)$  for the fractal grid.

erated by the fractal grid, while both contributions play a significant role in the case of the regular grid. Similar results are obtained for others observer locations.

From the previous pressure signals, we can obtain the spectra of the Sound Pressure Level (SPL) at the corresponding observer location, defined as  $SPL = 10 \log \frac{p_g^2}{p_0^2}$ , with the reference value  $p_0 = 2 \cdot 10^{-5}$  Pa in standard atmospheric conditions. Figure 9 makes a comparison between the spectra obtained for both flows, where the spectra corresponding to the fractal square grid and the regular grid are the red curve and the blue dashed curve respectively. For low Strouhal numbers ( $St < 0.2$ , with  $St = ft_{min}/U_{\infty}$ ), the sound levels generated by the regular grid flow are larger than the sound levels generated by the fractal square grid flow. For higher Strouhal numbers ( $0.2 < St < 0.4$ ), the sound levels generated by the fractal grid flow are larger than the sound levels generated by the regular grid flow, while for the largest Strouhal numbers, both spectra seem quite similar. This trend is consistent with that obtained in laboratory experiments on the acoustic performance of fractal spoilers [2], even through the experimen-

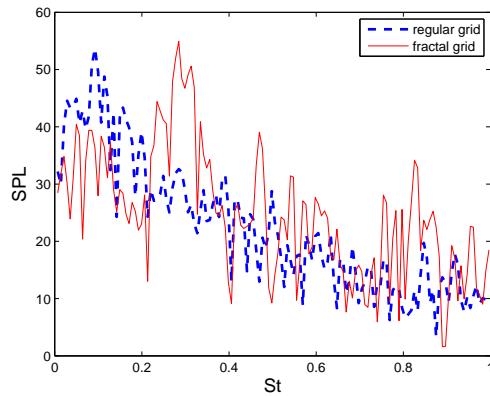


Figure 9. Comparison of acoustic spectra measured at the observer location ( $250 t_{min}, 433 t_{min}, 0$ ) for both grids (red curve: fractal grid, blue dashed curve: regular grid).

tal set-up was different and the fractal spoilers had a much higher blockage ratio ( $\sigma \approx 0.75$ ). In the experiments [2], the spectra of the fractal spoilers showed a reduction of the sound levels at lower frequencies similarly to what we observe here where there is a reduction for  $St \leq 0.2$ . Finally, we find that in present results, the overall noise generated by the fractal square grid flow is found to be slightly larger (1.5 dB) than the overall noise generated by the regular grid flow.

### Acknowledgements

The authors are grateful to Dr. Ning Li for helping with the parallel version of **Incompact3d** and David Froger for helping with the acoustic code. We also acknowledge support from EPSRC Research grants EP/E00847X/1 and EP/F051468/1 and we thank the DEISA Consortium ([www.deisa.eu](http://www.deisa.eu)), co-funded through the EU FP6 project RI-031513 and the FP7 project RI-222919, for support within the DEISA Extreme Computing Initiative.

### REFERENCES

- [1] J. Nedic, B. Ganapathisubramani, J. Vassilicos, J. Borée, L. Brizzi, and A. Spohn, “Aero-acoustic performance of fractal spoilers,” in *63rd Annual Meeting of the APS Division of Fluid Dynamics*, (Long Beach, USA), 2010.
- [2] J. Nedic, B. Ganapathisubramani, J. Vassilicos, J. Borée, L. Brizzi, and A. Spohn, “Aero-acoustic performance of fractal spoilers,” in *49th AIAA Aerospace Sciences Meeting Including The New Horizons Forum and Aerospace Exposition*, (Orlando, USA), 2011.
- [3] D. Hurst and J. C. Vassilicos, “Scalings and decay of fractal-generated turbulence,” *Phys. Fluids*, vol. **19**, no. 035103, 2007.
- [4] N. Mazellier and J. Vassilicos, “Turbulence without Richardson-Kolmogorov cascade,” *Phys. Fluids*, vol. **22**, no. 075101, 2010.
- [5] J. Freund, “Noise sources in a low-Reynolds-number turbulent jet at mach 0.9,” *J. Fluid Mech.*, vol. 438, pp. 277–305, 2001.

- [6] V. Fortuné, E. Lamballais, and Y. Gervais, “Noise radiated by a non-isothermal, temporal mixing layer. part i: Direct computation and prediction using compressible dns,” *Theoret. Comput. Fluid Dynamics*, vol. 18, pp. 61–81, 2003.
- [7] C. Bogey and C. Bailly, “Investigation of downstream and sideline subsonic jet noise using large eddy simulation,” *Theoret. Comput. Fluid Dynamics*, vol. 20(1), pp. 23–40, 2006.
- [8] M. Terracol, E. Manoha, C. Herrero, E. Labourasse, S. Redonnet, and P. Sagaut, “Hybrid methods for airframe noise numerical prediction,” *Theoret. Comput. Fluid Dynamics*, vol. 19(3), pp. 197–227, 2005.
- [9] E. Großchel, W. Schröder, P. Renze, M. Meinke, and P. Comte, “Noise prediction for a turbulent jet using different hybrid methods,” *Computers and Fluids*, vol. 37, pp. 416–426, 2008.
- [10] S. Laizet and J. Vassilicos, “Dns of fractal-generated turbulence,” *Flow, Turbulence and Combustion*, vol. In Press, 2011.
- [11] S. Laizet and E. Lamballais, “High-order compact schemes for incompressible flows: a simple and efficient method with the quasi-spectral accuracy,” *J. Comp. Phys.*, vol. **228(16)**, pp. 5989–6015, 2009.
- [12] S. Laizet, E. Lamballais, and J. Vassilicos, “A numerical strategy to combine high-order schemes, complex geometry and parallel computing for high resolution dns of fractal generated turbulence,” *Computers and Fluids*, vol. **39(3)**, pp. 471–484, 2010.
- [13] S. Laizet and N. Li, “Incompact3d, a powerful tool to tackle turbulence problems with up to ( $10^5$ ) computational cores,” *Int. J. Numer. Methods Fluids*, vol. DOI: 10.1002/fld.2480, 2011.
- [14] S. Laizet and J. C. Vassilicos, “Direct numerical simulation of fractal-generated turbulence,” in *Proc. DLES-7*, (Trieste), 2008.
- [15] M. J. Lighthill, “On sound generated aerodynamically I. General theory,” *Proc. Roy. Soc. A*, vol. 211, pp. 564–587, 1952.
- [16] N. Curle, “The influence of solid boundaries upon aerodynamic sound,” *Proc. Roy. Soc. of London*, vol. series A, 231, pp. 505–513, 1955.
- [17] X. Gloerfelt, F. Pérot, C. Bailly, and D. Juvé, “Flow-induced cylinder noise formulated as a diffraction problem for low Mach number,” *J. Sound Vib.*, vol. **287**, pp. 129–151, 2005.
- [18] F. Margnat and V. Fortuné, “An iterative algorithm for computing aeroacoustic integrals with application to the analysis of free shear flow noise,” *J. Acoust. Soc. Am.*, vol. **128(4)**, pp. 1656–1667, 2010.
- [19] D. Casalino, “An advanced time approach for acoustic analogy predictions,” *J. Sound Vib.*, vol. 261, pp. 583–612, 2003.
- [20] D. Froger, V. Fortuné, and E. Lamballais, “Acoustic analogy prediction using direct numerical simulation and immersed boundary method,” in *Ercofac colloquium on IBM : current status and future research directions*, (Amsterdam, The Netherlands), 2009.